remote sensing

Article

Erosion Associated with Seismically-Induced Landslides in the Middle Longmen Shan Region, Eastern Tibetan Plateau, China

Zhikun Ren [1,2,*], Zhuqi Zhang [2] and Jinhui Yin [2]

[1] Key Laboratory of Active Tectonics and Volcano, Institute of Geology, China Earthquake Administration, Beijing 100029, China

[2] State Key Laboratory of Earthquake Dynamics, Institute of Geology, China Earthquake Administration, Beijing 100029, China; zzqgeorge@gmail.com (Z.Z.); yjhdzs@ies.ac.cn (J.Y.)

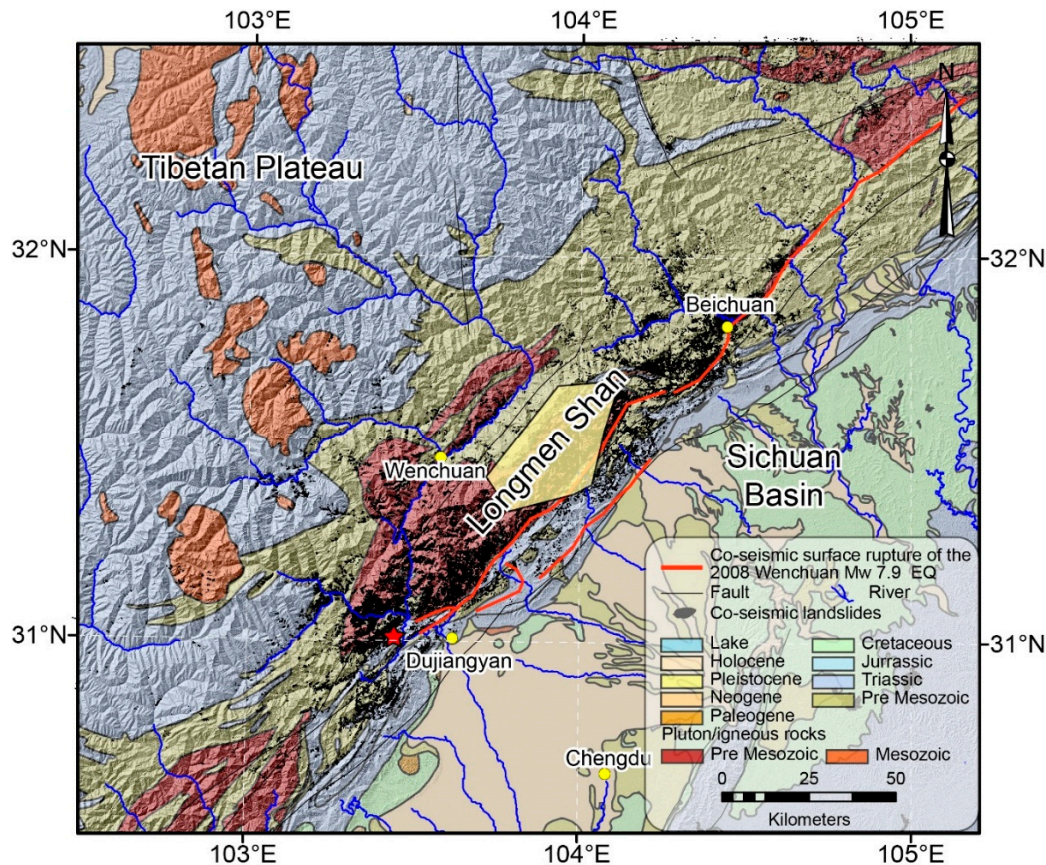[*] Correspondence: rzk@ies.ac.cn; Tel.: +86-010-6200-9044

Abstract: The 2008 Wenchuan earthquake and associated co-seismic landslide was the most recent expression of the rapid deformation and erosion occurring in the eastern Tibetan Plateau. The erosion associated with co-seismic landslides balances the long-term tectonic uplift in the topographic evolution of the region; however, the quantitative relationship between earthquakes, uplift, and erosion is still unknown. In order to quantitatively distinguish the seismically-induced erosion in the total erosion, here, we quantify the Wenchuan earthquake-induced erosion using the digital elevation model (DEM) differential method and previously-reported landslide volumes. Our results show that the seismically-induced erosion is comparable with the pre-earthquake short-term erosion. The seismically-induced erosion rate contributes ~50% of the total erosion rate, which suggests that the local topographic evolution of the middle Longmen Shan region may be closely related to tectonic events, such as the 2008 Wenchuan earthquake. We propose that seismically-induced erosion is a very important component of the total erosion, particularly in active orogenic regions. Our results demonstrate that the remote sensing technique of differential DEM provides a powerful tool for evaluating the volume of co-seismic landslides produced in intermountain regions by strong earthquakes.

Keywords: Wenchuan earthquake; topographic evolution; seismically-induced erosion; differential DEM

1. Introduction

Landscape evolution in active orogenic areas is influenced by both climate-driven denudation and tectonic processes [1,2]. It is widely accepted that large dip-slip or oblique-slip earthquakes are responsible for building high mountains and plateau regions [3,4]. The subsequent effects of strong earthquakes are believed to be very important in shaping the resultant landscape [4,5]; however, the role of erosion associated with strong earthquakes has not been quantitatively studied. The quantitative study of the role of co-seismic landslides is vital to our understanding of the relationship between earthquakes, landslides, and erosion [6–9], as well as the landscape evolution in tectonically-active mountain belts. The 2008 Mw 7.9 Wenchuan earthquake triggered numerous landslides, and provided a rare opportunity to study the geomorphic response to a strong earthquake (Figure 1). Due to the limitation of available data in previous studies, landslide volumes have typically been derived from landslide areas using statistical equations [4,10–13]. Researchers also tried using the spaceborne interferometric synthetic aperture radar (InSAR) [14] and remote sensing and digital terrain model (DTM) data [15] to evaluate mass wasting volume, but only concentrated on the giant Daguangbao

landslide. Parker et al. [4] suggested that the co-seismic landslide volume is much larger than the co-seismic uplift, thus challenging the role of strong earthquakes in mountain building. However, Li et al. [11] re-evaluated the co-seismic landslide volume based on the Monte Carlo distribution of lower and upper bounds by running random samplings of the scaling parameters 50,000 times, and showed that the total co-seismic landslide mass is comparable with the co-seismic uplift.

Figure 1. Simplified geological structures of the Longmen Shan region. Thick red lines indicate the co-seismic surface ruptures of the 2008 Mw 7.9 Wenchuan earthquake [16–18]. The gray polygons indicate the landslide inventory (courtesy of Joshua West and Gen Li), and the yellow polygon indicates the area covered by the high-resolution DEM.

The evolution of continental relief is controlled by multiple factors, including tectonic forcing and erosion [2,19–21]. The role of erosion on the morphological evolution of plateau margins has been widely reported [22–27]; however, the co-seismically-induced erosion associated with strong earthquakes has rarely been quantitatively reported. Most geomorphological studies [20,22,24,28–30] have focused on long-term erosion at the million-year scale, and short-term erosion rates at the thousand-year to decade scale. These erosion rates represent a combination of climatic erosion and seismically-induced erosion. However, erosion associated with landslides and earthquakes is also one of the most important influences on topographical evolution [29]. Thus, it is essential to understand the impact of erosion associated with landslides and earthquakes on long-term average erosion rates. The seismically-induced erosion could be considered as the mass balance of a strong earthquake, by removing the landslide materials [31]. A hypothetical erosion variation model which shows the erosion variation pattern associated with strong earthquakes was proposed by Ouimet [29]. In this model, the main variation in erosion rate is represented as a rapid increase in erosion rate associated with the occurrence of an earthquake, which then gradually returns to the pre-earthquake level during a seismic recurrence interval. A recent study by West et al. [32] suggests that the short-term and

modern erosion rates obtained before the Wenchuan earthquake are likely to be underestimating the long-term erosion. Thus, quantitatively comparing the seismically-induced erosion and cosmogenic or modern hydrological erosion will enhance our understanding of the role of earthquakes in erosion and geomorphic evolution. Usually, in geomorphological studies, the erosion rates are a mixture of natural erosion including human influence, earthquakes, etc., because it is difficult for us to distinguish the sources of erodible materials. The occurrence of the 2008 Mw 7.9 Wenchuan earthquake provides us with a rare opportunity to quantitatively study the earthquake-induced erosions and distinguish it from the total erosion. Although previous studies have reported the distribution of erosion rates in the eastern Tibetan Plateau [22,24,28,30], there are no detailed data from within the middle Longmen Shan region. In this study, we quantitatively study how co-seismic landslides, particularly those associated with strong earthquakes such as the 2008 Mw 7.9 Wenchuan earthquake, contribute to the long-term erosion of active orogenic regions.

2. Tectonic Setting

On the eastern margin of the Tibetan Plateau, the Longmen Shan orogenic belt trends NE–SW along the strike of the Longmen Shan Thrust Belt, which marks one of the steepest topographic margins of the plateau. Long-term convergence within the active Longmen Shan region has produced a steep topographic relief of 5000 m within the 50 km distance from the lowland Sichuan Basin to the inter-plateau region (Figure 1; [33–35]). The Longmen Shan Thrust Belt consists of three major fault systems: the Wenchuan-Maowen, Yingxiu-Beichuan, and Guanxian-Anxian fault systems [28,36–38]. There is a consensus that the Yingxiu-Beichuan and Guanxian-Anxian faults are the seismogenic faults associated with the 2008 Wenchuan earthquake [16–18]. Numerous co-seismic landslides were triggered due to the co-seismic deformation and strong ground motion along the rupture zone [4,11,25,39,40], influencing the local erosion rate as well as the topographic evolution.

The erosion rate increases after an earthquake, as the large amount of co-seismic landslide material associated with the earthquake is gradually transported out of the catchments by the rivers [4,7,8,10]. Recent studies reveal that the residence time of fine-grained sediment from co-seismic landslides associated with the Wenchuan earthquake ranges from one year to over a century [31]. Calculations based on [10]Be mixing proportions suggest that river sediment fluxes in the 2–3 years following the Wenchuan earthquake increased by a similar order of magnitude in the 0.25–1 mm and the <0.25 mm size fractions, determined from [10]Be quartz mixing calculations and hydrological gauging sand, respectively [32]. During the inter-seismic period, the erosion rate will then gradually return to the pre-earthquake level [29].

In this study, we use the pre- and post-earthquake digital elevation models (DEM) to derive the co-seismic landslide volume and to calculate the amount of seismically-induced erosion at one typical region within the Longmen Shan region [26]. We also compare the amount of erosion obtained from the differential DEM method with previous results of landslide volumes proposed by Li et al. [11].

3. Data and Methods

In this study, we estimated the seismically-induced erosion associated with landslides using the DEM differential method [26] and the landslide volume information from Li et al. [11].

Analysis of pre- and post-earthquake DEM data can be used to obtain elevation change information, which can then be used to detect co-seismic deformation [41]. Here, we use the DEM differential method [26] to calculate the minimum landslide volume within the landslide area by subtracting the pre-earthquake DEM from the post-earthquake DEM. In the middle Longmen Shan region, one typical site (near the Pengguan Massif) was selected to derive the pre- and post-earthquake DEM. There are no high-resolution DEMs available before the Wenchuan earthquake. The best pre-earthquake DEM has a resolution of 25 m and has been derived from digital 1:50,000 topographic maps, which were surveyed from stereo pairs of aerial photographs in the 1970s by the National Administration of Surveying, Mapping, and Geoinformation of China. By comparing the

pre-earthquake DEM elevation with 14 continuous GPS observation sites, a mean elevation error of ±4.1 m, and a median error of ±3.6 m were determined [26]. In the error analysis, the median error is most appropriate in describing the level of elevation error [42] because the distribution of the elevation errors is not precisely known.

In this study, a 5-m resolution post-earthquake DEM was derived from 2.5-m resolution stereo pairs taken from Indian Remote Sensing Satellite P5 (IRS-P5) images (Table 1). The data were acquired three weeks after the 12 May Wenchuan earthquake in 2008, with almost no cloud [26,27]. In order to improve the quality of the post-earthquake DEM, we also applied a field ground control points (GCP) survey using Trimble R8 GPS for at least 15 min at each point (Figure 1), with a continuous reference station within a range of 50 km. The post-earthquake DEM data is derived using the ground control points and tie points between the Pan fore and Pan after imagery, by applying the rational polynomial coefficient (RPC) camera model [43]. The elevation error of the post-earthquake DEM is obtained by comparing the DEM with 12 field GPS observations spanning approximately ~15–30 min. The observation error of the GPS survey is less than several centimeters [44]. The mean elevation error is estimated to be ±1.5 m, and the median error is estimated to be ±1.2 m [26]. Thus, it is reasonable to estimate the minimum landslide volume (volume of large and deep-seated landslides) using the co-seismic elevation change [26]. In order to obtain a higher resolution and, thus, more reliable results, we first smoothed the post-earthquake DEM data to the same resolution of 25 m as pre-earthquake DEM. The co-seismic elevation change is derived by the subtraction of the pre- from the post-earthquake DEMs, and the minimum landslide volume is calculated by summing up the total volume change within the landslide area. Although our pre-earthquake DEM data is not of as high a resolution as the post-earthquake DEM data, it is possible to derive an estimate of the volume information of large and deep-seated landslides.

Table 1. Stereo pairs IRS-P5 Imagery used in post-earthquake DEM derivation.

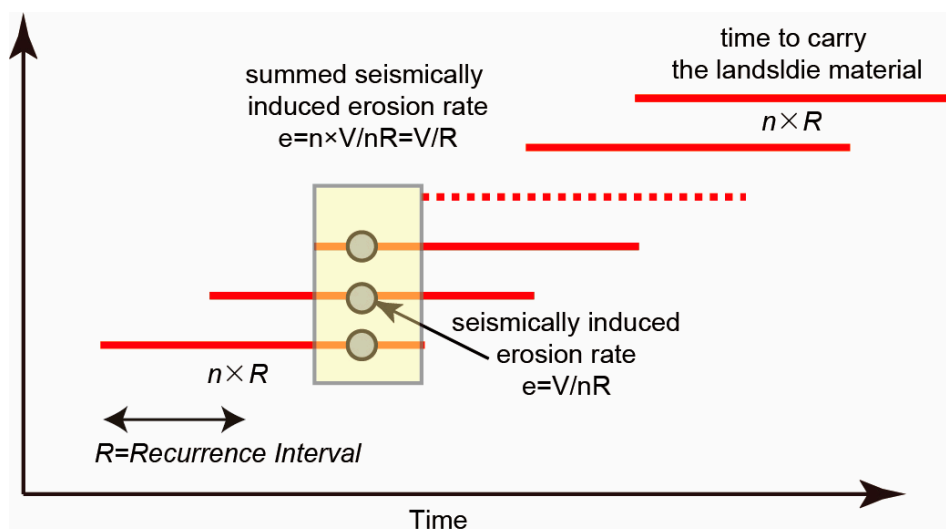| No.	Path	Row	Date	Resolution (m)
1	659	250	20080603	
2	659	251	20080603	
3	659	252	20080603	2.5
4	659	253	20080603	
5	659	254	20080603	

4. Results

4.1. Landslide Volume

All landslide volumes within the typical site in the middle Longmen Shan region [26] are derived from the elevation differences between the pre-and post-earthquake DEM; areas are confined using the landslide inventory of Dai et al. [40]. Negative and positive values represent the elevation change in landslide and deposition regions, respectively. The landslide volume is calculated by summing up the negative elevation change within the landslide area in each catchment, which is the minimum volume because the co-seismic deformation is also involved. However, the co-seismic deformation within the deep-seated landslide region is small when compared with the elevation change due to landslide activity. Thus, it is reasonable to use this data to estimate the average seismically-induced erosion rate because the deep landslides are the major contributor to landslide volume whose depth is much larger than the co-seismic uplift. The error represents the volume uncertainties due to the error of DEM data. Uncertainty in landslide volume leads to variability in the seismically-induced erosion, but the variability in seismically-induced erosion is generally less than 1/107 of the landslide volume. Additionally, the variability induced by uncertainty in the landslide volume has little influence on the spatial pattern of seismically-induced erosion. Since we study the spatial distribution of the

seismically-induced erosion, the degree of uncertainty in landslide volumes will not alter the spatial distribution of the seismically-induced erosion.

To reveal the details of seismically-induced erosion within the middle Longmen Shan region, we derived small catchments to analyze the detailed distribution features of the seismically-induced erosion within the study area. The landslide volumes within each catchment are derived from the landslide distribution and volume information from Li et al. [11], and then summed up within each catchment.
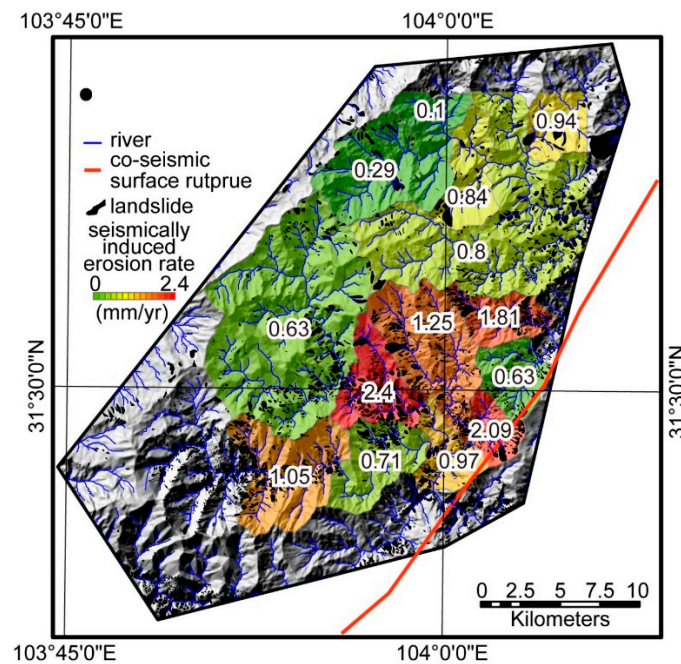
4.2. Erosion Rate

The average erosion depth is calculated by dividing the summed landslide volume by the corresponding catchment area. A recent study by Wang et al. [31] suggests that the fine-grained sediment from co-seismic landslides associated with the Wenchuan earthquake will be transported out of the Longmen Shan region within timescales ranging from one year to over a century. Although we do not know the precise timescale required for the landslide material to be totally removed from the catchment area, the summed seismically-induced erosion rate 'e' can be assumed to be equal to V/R (Figure 2), where 'R' is the recurrence interval of a Wenchuan-like earthquake, and 'V' is the volume of the landslide material. Thus, if the landslide material is transported out of the catchment within a single recurrence interval of 'R', then the seismically-induced erosion rate will be e = V/R. If the removal of the landslide material takes several recurrence intervals, nR, then after each earthquake, there will be a seismically-induced erosion rate of V/nR. However, during each recurrence interval, the summed seismically-induced erosion rate will also be V/R (Figure 2), hence, it is reasonable to assume the seismically-induced erosion rate to be V/R.
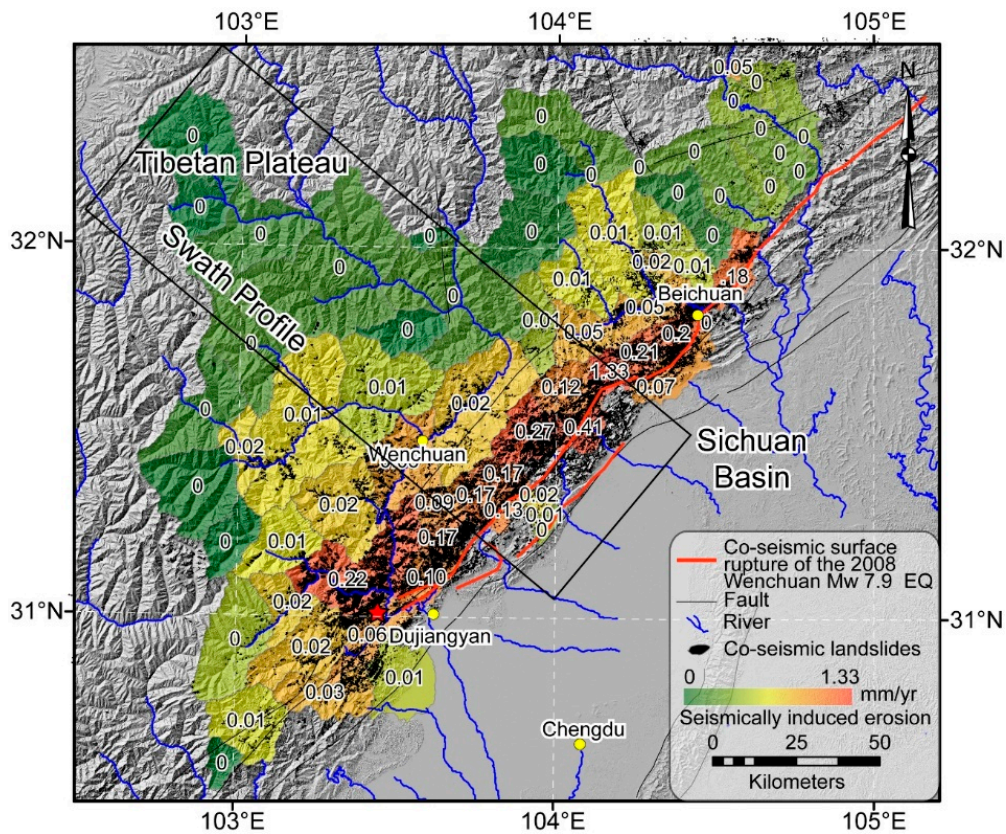

Figure 2. Simplified comparison of erosion rates according to the residence time of the co-seismic landslide material.

In this study, we used a recurrence interval of 2000–3000 years (much longer than the estimated residence time of fine-grained sediment), determined from Global Positining System (GPS) and paleoseismological data (Figure 3) [45–47]. The seismically-induced erosion rates (E_{Max} and E_{Min}) are calculated using the recurrence interval of 2000 and 3000 years, respectively. The mean seismically-induced erosion rate (E_{ave}) is the mean value of E_{Max} and E_{Min}.

Figure 3. The seismically-induced erosion rates derived using the differential DEM method shown within the area covered by the high-resolution DEM. Erosion rates are calculated within small catchments by summing up the landslide volume using the elevation difference.

The average seismically-induced erosion rates within small catchments, calculated using the differential DEM method, range from 0.1–2.4 mm/year (Figure 3, Table 2). Within larger catchments, the average seismically-induced erosion rates are derived from landslide volumes of Li et al., and range from 0–1.3 mm/year (Figure 4, Table 3). The distribution of erosion rates within the small catchments reveals that the seismically-induced erosion rates are not homogeneous and that high erosion rates are mainly focused in a narrow corridor near the co-seismic surface rupture zone (Figures 3 and 4). These high seismically-induced erosion rates are typically not included when calculating the short-term erosion rate. The long-term erosion rate is an averaged erosion rate, calculated by averaging all the landslide erosion within numerous recurrence intervals, and is therefore typically higher than the short-term erosion rate [22,32]. Our studies suggest that the average seismically-induced erosion within the Longmen Shan region is ~0.4 mm/year with a maximum value of ~1.3 mm/year (Figure 4). The average pre-earthquake erosion derived from hydrometric stations is ~0.5 mm/year [24], with a maximum value of ~1.0 mm/year, calculated from [10]Be dating [22]. A simple comparison indicates that seismically-induced erosion contributes ~50% to the total erosion. The erosion distribution also indicates that the seismically-induced erosion is mainly focused in the Longmen Shan region, and that seismically-induced erosion within the Tibetan Plateau is almost zero.

Figure 4. The seismically-induced erosion rates within each catchment in the Longmen Shan region. Erosion rates are calculated using the summed landslide volumes within each catchment.

Table 2. Seismically-induced erosion rates calculated using the differential DEM method within each catchment shown in Figure 3.

Catchment Area (1×10^6 m^2)	Sum Volume (1×10^6 m^3)	Average Erosion (m)	E_{Max} (mm/year)	E_{Min} (mm/year)	E_{ave} (mm/year)	E_{error} (mm/year)
10.06	2.51 ± 0.11	0.25	0.12	0.08	0.1	0.02
15.03	33.97 ± 1.82	2.26	1.13	0.75	0.94	0.19
41.97	29.50 ± 2.84	0.71	0.35	0.23	0.29	0.06
19.62	39.21 ± 2.58	2.00	1.00	0.67	0.84	0.17
94.66	182.12 ± 1.17	1.92	0.96	0.64	0.8	0.16
15.98	69.31 ± 5.41	4.34	2.17	1.45	1.81	0.36
16.61	24.82 ± 2.30	1.49	0.75	0.50	0.63	0.13
23.12	133.00 ± 7.55	5.75	2.88	1.92	2.4	0.48
39.73	119.08 ± 7.76	3.00	1.50	1.00	1.25	0.25
109.11	163.27 ± 0.35	1.50	0.75	0.50	0.63	0.13
11.27	56.14 ± 3.07	4.98	2.50	1.67	2.09	0.42
15.15	35.08 ± 3.29	2.32	1.16	0.77	0.97	0.20
23.73	40.34 ± 3.33	1.70	0.85	0.57	0.71	0.14
37.46	94.62 ± 8.28	2.53	1.26	0.84	1.05	0.21

E_{max} means the maximum erosion rate, E_{min} means the minimums erosion rate, E_{ave} means the average erosion rate and E_{error} means the errors of the erosion rate.

Table 3. Seismically-induced erosion rates derived from the landslide volume data of Li et al. [11] within each of the catchments shown in Figure 4.

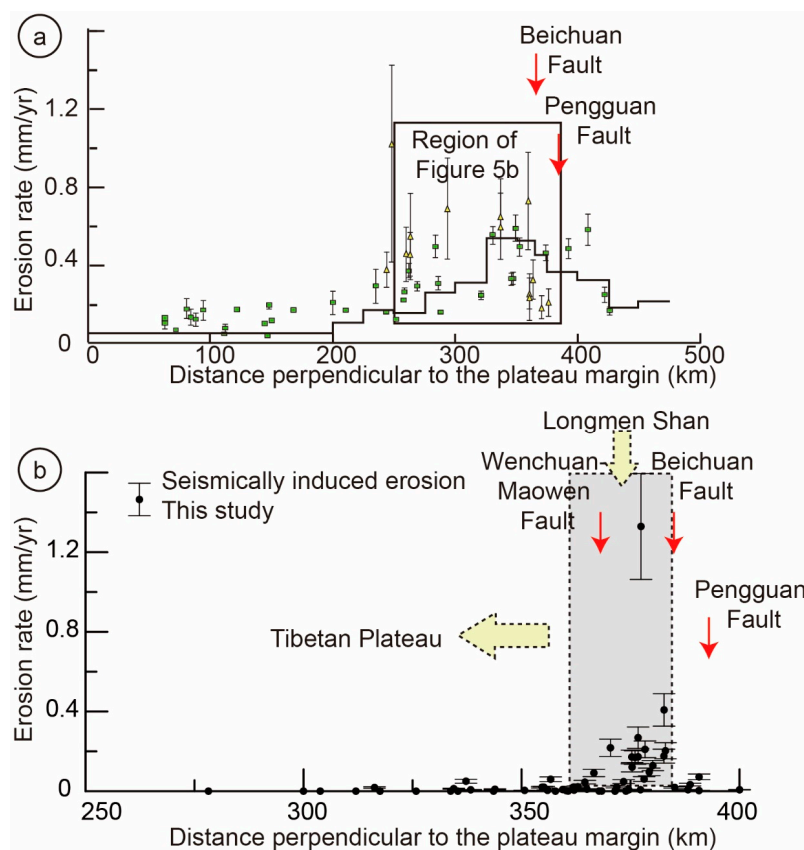| Catchment Area (1 × 10^6 m²)	Sum Volume (1 × 10^6 m³)	Average Erosion (m)	E_{Max} (mm/year)	E_{Min} (mm/year)	E_{ave} (mm/year)	E_{error} (mm/year)
124.19	3.96	3.19	1.60	1.06	1.33	0.27
131.45	1.29	0.98	0.49	0.33	0.41	0.08
310.04	2.00	0.64	0.32	0.21	0.27	0.05
685.05	3.58	0.52	0.26	0.17	0.22	0.04
144.67	0.73	0.50	0.25	0.17	0.21	0.04
134.13	0.65	0.49	0.24	0.16	0.20	0.04
282.31	1.19	0.42	0.21	0.14	0.18	0.04
124.54	0.52	0.41	0.21	0.14	0.17	0.03
130.21	0.54	0.41	0.21	0.14	0.17	0.03
128.79	0.52	0.41	0.20	0.14	0.17	0.03
88.53	0.27	0.31	0.15	0.10	0.13	0.03
245.31	0.71	0.29	0.14	0.10	0.12	0.02
197.02	0.46	0.23	0.12	0.08	0.10	0.02
129.22	0.28	0.22	0.11	0.07	0.09	0.02
244.69	0.42	0.17	0.09	0.06	0.07	0.01
272.35	0.40	0.15	0.07	0.05	0.06	0.01
459.91	0.66	0.14	0.07	0.05	0.06	0.01
30.16	0.04	0.12	0.06	0.04	0.05	0.01
251.97	0.29	0.11	0.06	0.04	0.05	0.01
249.58	0.27	0.11	0.05	0.04	0.05	0.01
327.19	0.26	0.08	0.04	0.03	0.03	0.01
52.69	0.03	0.05	0.03	0.02	0.02	0.00
445.14	0.22	0.05	0.03	0.02	0.02	0.00
808.06	0.39	0.05	0.02	0.02	0.02	0.00
514.30	0.25	0.05	0.02	0.02	0.02	0.00
220.88	0.11	0.05	0.02	0.02	0.02	0.00
65.27	0.03	0.05	0.02	0.02	0.02	0.00
187.41	0.08	0.04	0.02	0.01	0.02	0.00
1063.00	0.33	0.03	0.02	0.01	0.01	0.00
613.53	0.15	0.02	0.01	0.01	0.01	0.00
346.56	0.08	0.02	0.01	0.01	0.01	0.00
332.62	0.07	0.02	0.01	0.01	0.01	0.00
394.67	0.07	0.02	0.01	0.01	0.01	0.00
18.42	0.00	0.02	0.01	0.01	0.01	0.00
129.69	0.02	0.02	0.01	0.01	0.01	0.00
394.32	0.07	0.02	0.01	0.01	0.01	0.00
692.51	0.11	0.02	0.01	0.01	0.01	0.00
212.18	0.03	0.01	0.01	0.00	0.01	0.00

5. Discussion

The correlation between the erosion rate and topography is central to our understanding of the controls on sediment flux, and of the feedback between tectonics, climate, and erosion in shaping topography [21,48]. In this study, we show the detailed distribution of seismically-induced erosion due to the 2008 Wenchuan earthquake and quantitatively analyze how it has influenced long-term erosion in the region.

In geomorphic studies, long-term erosion typically refers to erosion occurring over million-year timescales, and short-term erosion refers to erosion over timescales ranging from tens to thousands of years. Erosion rates at the thousand-year timescale typically represent non-seismically-induced erosion, and are derived using cosmogenic dating methods, such as ^{10}Be and ^{26}Al. In contrast, decadal erosion rates are derived from sediment load data recorded by hydrographic gauge stations, and may not include seismically-induced erosion. These data are collected prior to 2008, almost at the end of the inter-event time between the prior earthquake and the 2008 Wenchuan earthquake; hence, these erosion rates do not appear to be affected by the co-seismic landslides of both the 2008 Wenchuan and prior earthquakes. Meanwhile, for the purposes of geomorphic study, erosion data is usually collected so as to avoid or minimize the influence of landslides, particularly co-seismic landslides.

The results from a number of previous studies, utilizing a variety of data and techniques, suggest high erosion rates along the plateau margin: e.g., Kirby et al. [28] calculated long-term erosion rates

using low-thermochronology dating, Godard et al. [22] and Ouimet et al. [30] calculated short-term erosion rates using ^{10}Be and ^{26}Al dating, and Liu-Zeng et al. [24] calculated modern erosion from hydrological gauge data. Consequently, we can conclude that high erosion rates are primarily focused in a narrow strip (200 km in width) along the plateau margin and the region bounding the Longmen Shan Thrust Belt. High seismically-induced erosion rates are due to a high concentration of co-seismic landslides, thus, such high erosion rates will occur predominantly in the regions bounding the fault zone, especially the hanging wall near the co-seismic surface rupture. Our results reveal that the high seismically-induced erosion rates are further concentrated within a narrow corridor bounding the Longmen Shan (~50 km in width) within the previously-demonstrated high denudation zone (Figure 5). It is difficult for us to distinguish the sources of erodible materials, hence, we could only compare the erosion associated with co-seismic landslides and the total natural erosion. Our results reveal that the erosion associated with co-seismic landslides contributes ~50% to the total natural erosion rate within the middle Longmen Shan region.

Figure 5. (**a**) Distribution of short-term erosion rates from previous studies (modified from Reference [24]) and (**b**) seismically- induced erosion rates from this study.

Our results also reveal that the erosion rates distribution was additionally affected by the size of the catchment. The uncertainties of our study indicate that the variability in seismically-induced erosion is generally less than 1/107 of the landslide volume, which also has little influence on the spatial pattern of seismically-induced erosion. The highest seismically-induced erosion rate is ~2.4 mm/year (Figure 3), while the average erosion rate is ~0.7 mm/year, derived from catchments with an average area of ~30 km^2 (Table 2). The highest erosion rate in the largest catchment covered by the high-resolution DEM data is ~0.41 mm/year (Figure 4, Table 3), derived from catchments with an average area of ~300 km^2, which is 10 times larger than the catchment size used in the differential DEM method. Previously-reported erosion rates in the Longmen Shan region have been calculated

using different methods and sizes of catchments. The erosion rates from Ouimet et al. [30] were derived from small catchments (several tens of km^2) using cosmogenic dating; in contrast, the erosion rates of Liu-Zeng et al. [24] were derived from large catchments (hundreds to thousands of km^2) using hydrological gauge data. The erosion rates from Kirby et al. [28] were roughly estimated using sparsely-distributed low-thermochronological dating results. Thus, when using these erosion rates, we need to consider the size of the catchment, as well as the method used to derive them. Erosion rates derived from larger catchments or regions could reveal large-scale features of regional evolution of the plateau margins [24,28], whereas erosion rates derived from smaller catchments, such as those in this study, may reveal smaller-scale detailed features of the topographic evolution within the Longmen Shan fault zone.

6. Conclusions

In order to quantitatively analyze the contribution from seismically-induced erosion to the topographic erosion in the Longmen Shan region, we have distinguished the seismically-induced erosion from the total erosion and quantitatively compared the seismically-induced erosion, short-term erosion, and long-term erosion rates. The results show that earthquake-triggered erosion has played an important role in shaping the landscape in the middle Longmen Shan region. The comparison indicates that the seismically-induced erosion contributes ~50% of the long-term erosion, which is comparable with the shorter-term erosion (Figure 5). If the seismically-induced erosion could account for ~50% of the long-term erosion, then the topographic evolution in the Longmen Shan region should be closely related to repeated tectonic events, such as the 2008 Wenchuan earthquake. Thus, in tectonically-active mountain ranges, erosion associated with strong earthquakes will play a major role in controlling the landscape evolution.

Based on a comparison of the pre- and post-Wenchuan earthquake topography, previous study also demonstrated that the slope and roughness are closely related to large tectonic events, such as the Wenchuan earthquake [26]. Thus, in conclusion, the role of seismically-induced erosion cannot be ignored in geomorphic studies, particularly in active orogenic regions. Our results also demonstrate that differential DEM is a powerful remote sensing technique for the evaluation of the volume of co-seismic landslides produced in intermountain regions by strong earthquakes.

Author Contributions: Z. Ren contributed to conceiving the idea, prepared the figures, data compilation, and wrote the manuscript text. Z. Ren, Z. Zhang, and J. Yin discussed the contents of the manuscript.

Conflicts of Interest: Competing financial interests: The authors declare no competing financial interests.

References

1. Avouac, J.P. Dynamic processes in extensional and compressional settings-mountain building. In *Treatise on Geophysics*; Watts, A.B., Ed.; Elsevier: Amsterdam, The Netherlands, 2008; Volume 6, pp. 377–439.
2. Burbank, D.W.; Anderson, R.S. *Tectonic Geomorphology*; Blackwell Science: Cambridge, MA, USA, 2012; p. 454.
3. Hovius, N.; Meunier, P.; Lin, C.-W.; Chen, H.; Chen, Y.-G.; Dadson, S.; Horng, M.-J.; Lines, M. Prolonged seismically induced erosion and the mass balance of a large earthquake. *Earth Planet. Sci. Lett.* **2011**, *304*, 347–355. [CrossRef]
4. Parker, R.N.; Densmore, A.L.; Rosser, N.J.; de Michele, M.; Li, Y.; Huang, R.; Whadcoat, S.; Petley, D.N. Mass wasting triggered by the 2008 wenchuan earthquake is greater than orogenic growth. *Nat. Geosci.* **2011**, *4*, 449–452. [CrossRef]
5. Korup, O.; Densmore, A.L.; Schlunegger, F. The role of landslides in mountain range evolution. *Geomorphology* **2010**, *120*, 77–90. [CrossRef]

6.   Dadson, S.J.; Hovius, N.; Chen, H.; Dade, W.B.; Lin, J.-C.; Hsu, M.-L.; Lin, C.-W.; Horng, M.-J.; Chen, T.-C.; Milliman, J.; et al. Earthquake-triggered increase in sediment delivery from an active mountain belt. *Geology* **2004**, *32*, 733–736. [CrossRef]

7.   Keefer, D.K. The importance of earthquake-induced landslides to long-term slope erosion and slope-failure hazards in seismically active regions. *Geomorphology* **1994**, *10*, 265–284. [CrossRef]

8.   Malamud, B.D.; Turcotte, D.L.; Guzzetti, F.; Reichenbach, P. Landslides, earthquakes, and erosion. *Earth Planet. Sci. Lett.* **2004**, *229*, 45–59. [CrossRef]

9.   Meunier, P.; Hovius, N.; Haines, A.J. Regional patterns of earthquake-triggered landslides and their relation to ground motion. *Geophys. Res. Lett.* **2007**, *34*. [CrossRef]

10. Larsen, I.J.; Montgomery, D.R.; Korup, O. Landslide erosion controlled by hillslope material. *Nat. Geosci.* **2010**, *3*, 247–251. [CrossRef]

11. Li, G.; West, A.J.; Densmore, A.L.; Jin, Z.; Parker, R.N.; Hilton, R.G. Seismic mountain building: Landslides associated with the 2008 wenchuan earthquake in the context of a generalized model for earthquake volume balance. *Geochem. Geophys. Geosyst.* **2014**, *15*, 833–844. [CrossRef]

12. Xu, C.; Xu, X.; Gorum, T.; van Westen, C.J.; Fan, X. Did the 2008 Wenchuan earthquake lead to a net volume loss? In *Landslide Science for a Safer Geoenvironment: Volume 3: Targeted Landslides*; Sassa, K., Canuti, P., Yin, Y., Eds.; Springer International Publishing: Cham, Switzerland, 2014; pp. 191–196.

13. Xu, C.; Xu, X.; Shen, L.; Yao, Q.; Tan, X.; Kang, W.; Ma, S.; Wu, X.; Cai, J.; Gao, M.; et al. Optimized volume models of earthquake-triggered landslides. *Sci. Rep.* **2016**, *6*, 29797. [CrossRef] [PubMed]

14. Chen, Q.; Cheng, H.; Yang, Y.; Liu, G.; Liu, L. Quantification of mass wasting volume associated with the giant landslide daguangbao induced by the 2008 Wenchuan earthquake from persistent scatterer insar. *Remote Sens. Environ.* **2014**, *152*, 125–135. [CrossRef]

15. Chen, Z.; Zhang, B.; Han, Y.; Zuo, Z.; Zhang, X. Modeling accumulated volume of landslides using remote sensing and dtm data. *Remote Sens.* **2014**, *6*, 1514–1537. [CrossRef]

16. Lin, A.; Ren, Z.; Jia, D.; Wu, X. Co-seismic thrusting rupture and slip distribution produced by the 2008 mw 7.9 wenchuan earthquake, china. *Tectonophysics* **2009**, *471*, 203–215. [CrossRef]

17. Liu-Zeng, J.; Zhang, Z.; Wen, L.; Tapponnier, P.; Sun, J.; Xing, X.; Hu, G.; Xu, Q.; Zeng, L.; Ding, L.; et al. Co-seismic ruptures of the 12 may 2008, ms 8.0 wenchuan earthquake, sichuan: East–west crustal shortening on oblique, parallel thrusts along the eastern edge of tibet. *Earth Planet. Sci. Lett.* **2009**, *286*, 355–370. [CrossRef]

18. Xu, X.; Wen, X.; Yu, G.; Chen, G.; Klinger, Y.; Hubbard, J.; Shaw, J. Coseismic reverse- and oblique-slip surface faulting generated by the 2008 Mw 7.9 wenchuan earthquake, China. *Geology* **2009**, *37*, 515–518. [CrossRef]

19. Burbank, D.W.; Blythe, A.E.; Putkonen, J.; Pratt-Sitaula, B.; Gabet, E.; Oskin, M.; Barros, A.; Ojha, T.P. Decoupling of erosion and precipitation in the Himalayas. *Nature* **2003**, *426*, 652–655. [CrossRef] [PubMed]

20. Godard, V.; Cattin, R.; Lavé, J. Erosional control on the dynamics of low-convergence rate continental plateau margins. *Geophys. J. Int.* **2009**, *179*, 763–777. [CrossRef]

21. Montgomery, D.R.; Brandon, M.T. Topographic controls on erosion rates in tectonically active mountain ranges. *Earth Planet. Sci. Lett.* **2002**, *201*, 481–489. [CrossRef]

22. Godard, V.; Lavé, J.; Carcaillet, J.; Cattin, R.; Bourlès, D.; Zhu, J. Spatial distribution of denudation in Eastern Tibet and regressive erosion of plateau margins. *Tectonophysics* **2010**, *491*, 253–274. [CrossRef]

23. Kirby, E.; Ouimet, W. Tectonic geomorphology along the eastern margin of Tibet: Insights into the pattern and processes of active deformation adjacent to the Sichuan basin. *Geol. Soc. Lond. Spec. Publ.* **2011**, *353*, 165–188. [CrossRef]

24. Liu-Zeng, J.; Wen, L.; Oskin, M.; Zeng, L. Focused modern denudation of the Longmen Shan margin, eastern Tibetan Plateau. *Geochem. Geophys. Geosyst.* **2012**, *12*. [CrossRef]

25. Ren, Z.; Lin, A. Co-seismic landslides induced by the 2008 Wenchuan magnitude 8.0 earthquake, as revealed by alos prism and avnir2 imagery data. *Int. J. Remote Sens.* **2010**, *31*, 3479–3493. [CrossRef]

26. Ren, Z.; Zhang, Z.; Dai, F.; Yin, J.; Zhang, H. Topographic changes due to the 2008 Mw 7.9 Wenchuan earthquake as revealed by the differential dem method. *Geomorphology* **2014**, *217*, 122–130. [CrossRef]

27. Ren, Z.; Zhang, Z.; Yin, J.; Dai, F.; Zhang, H. Morphogenic uncertainties of the 2008 Wenchuan earthquake: Generating or reducing? *J. Earth Sci.* **2014**, *25*, 668–675. [CrossRef]

28. Kirby, E.; Reiners, P.W.; Krol, M.A.; Whipple, K.X.; Hodges, K.V.; Farley, K.A.; Tang, W.; Chen, Z. Late cenozoic evolution of the eastern margin of the Tibetan Plateau: Inferences from 40ar/39ar and (u-th)/he thermochronology. *Tectonics* **2002**, *21*. [CrossRef]

29. Ouimet, W.B. Landslides associated with the May 12, 2008 Wenchuan earthquake: Implications for the erosion and tectonic evolution of the Longmen Shan. *Tectonophysics* **2010**, *491*, 244–252. [CrossRef]

30. Ouimet, W.B.; Whipple, K.X.; Granger, D.E. Beyond threshold hillslopes: Channel adjustment to base-level fall in tectonically active mountain ranges. *Geology* **2009**, *37*, 579–582. [CrossRef]

31. Wang, J.; Jin, Z.; Hilton, R.G.; Zhang, F.; Densmore, A.L.; Li, G.; West, A.J. Controls on fluvial evacuation of sediment from earthquake-triggered landslides. *Geology* **2015**, *43*, 115–118. [CrossRef]

32. West, A.J.; Hetzel, R.; Li, G.; Jin, Z.; Zhang, F.; Hilton, R.G.; Densmore, A.L. Dilution of 10Be in detrital quartz by earthquake-induced landslides: Implications for determining denudation rates and potential to provide insights into landslide sediment dynamics. *Earth Planet. Sci. Lett.* **2014**, *396*, 143–153. [CrossRef]

33. Burchfiel, B.C.; Zhiliang, C.; Yupinc, L.; Royden, L.H. Tectonics of the Longmen Shan and adjacent regions, central China. *Int. Geol. Rev.* **1995**, *37*, 661–735. [CrossRef]

34. Chen, S.F.; Wilson, C.J.L. Emplacement of the Longmen Shan thrust—Nappe belt along the eastern margin of the Tibetan Plateau. *J. Struct. Geol.* **1996**, *18*, 413–430. [CrossRef]

35. Deng, Q.D.; Chen, S.F.; Zhao, X.L. Tectonics, seismicity and dynamics of Longmenshan Mountains and its adjacent regions. *Seismol. Geol.* **1994**, *16*, 14.

36. Densmore, A.L.; Ellis, M.A.; Li, Y.; Zhou, R.; Hancock, G.S.; Richardson, N. Active tectonics of the Beichuan and Pengguan faults at the eastern margin of the Tibetan Plateau. *Tectonics* **2007**, *26*. [CrossRef]

37. Jia, D.; Wei, G.; Chen, Z.; Li, B.; Zeng, Q.; Yang, G. Longmen Shan fold-thrust belt and its relation to the western Sichuan Basin in central China: New insights from hydrocarbon exploration. *AAPG Bull.* **2006**, *90*, 1425–1447. [CrossRef]

38. Kirby, E.; Whipple, K.; Harkins, N. Topography reveals seismic hazard. *Nat. Geosci.* **2008**, *1*, 485–487. [CrossRef]

39. Dai, F.C.; Tu, X.B.; Xu, C.; Gong, Q.M.; Yao, X. Rock avalanches triggered by oblique-thrusting during the 12 May 2008 Ms 8.0 Wenchuan earthquake, China. *Geomorphology* **2011**, *132*, 300–318. [CrossRef]

40. Dai, F.C.; Xu, C.; Yao, X.; Xu, L.; Tu, X.B.; Gong, Q.M. Spatial distribution of landslides triggered by the 2008 Ms 8.0 Wenchuan earthquake, China. *J. Asian Earth Sci.* **2011**, *40*, 883–895. [CrossRef]

41. Cowgill, E.; Bernardin, T.S.; Oskin, M.E.; Bowles, C.; Yıkılmaz, M.B.; Kreylos, O.; Elliott, A.J.; Bishop, S.; Gold, R.D.; Morelan, A.; et al. Interactive terrain visualization enables virtual field work during rapid scientific response to the 2010 Haiti earthquake. *Geosphere* **2012**, *8*, 787–804. [CrossRef]

42. Bohm, G.; Zech, G. *Introduction to Statistics and Data Analysis for Physicists*; Deutsches Elekstrone-Synchrotron: Hamburg, Germany, 2010.

43. Tao, C.V.; Hu, Y. A comprehensive study of the rational function model for photogrammetric processing. *Anglais* **2001**, *67*, 10.

44. Gao, C.; Chen, A.; Chen, M.; Wang, X. Test and analysis for precision of gps precise point positioning. *J. Chin. Inert. Technol.* **2006**, *14*, 23–26.

45. Ran, Y.-K.; Chen, W.-S.; Xu, X.-W.; Chen, L.-C.; Wang, H.; Yang, C.-C.; Dong, S.-P. Paleoseismic events and recurrence interval along the Beichuan–Yingxiu fault of longmenshan fault zone, Yingxiu, Sichuan, China. *Tectonophysics* **2014**, *584*, 81–90. [CrossRef]

46. Shen, Z.-K.; Sun, J.; Zhang, P.; Wan, Y.; Wang, M.; Burgmann, R.; Zeng, Y.; Gan, W.; Liao, H.; Wang, Q. Slip maxima at fault junctions and rupturing of barriers during the 2008 Wenchuan earthquake. *Nat. Geosci.* **2009**, *2*, 718–724. [CrossRef]

47. Zhang, P.; Wen, X.; Shen, Z.; Chen, J. Oblique, high-angle, listric-reverse faulting and associated development of strain: The Wenchuan earthquake of May 12, 2008, Sichuan, China. *Annu. Rev. Earth Planet. Sci.* **2010**, *38*, 353–382. [CrossRef]

48. Whipple, K.X.; Kirby, E.; Brocklehurst, S.H. Geomorphic limits to climate-induced increases in topographic relief. *Nature* **1999**, *401*, 39–43. [CrossRef]